Direct observation of transverse and vortex metastable magnetic domains in cylindrical nanowires

C. Bran,[1,*] J. A. Fernandez-Roldan,[1] E. M. Palmero,[1,†] E. Berganza,[1] J. Guzman,[1] R. P. del Real,[1] A. Asenjo,[1] A. Fraile Rodríguez,[2,3] M. Foerster,[4] L. Aballe,[4] O. Chubykalo-Fesenko,[1] and M. Vazquez[1]

[1]*Institute of Materials Science of Madrid, CSIC, 28049 Madrid, Spain*

[2]*Departament de Física de la Matèria Condensada, Universitat de Barcelona, 08028 Barcelona, Spain*

[3]*Institut de Nanociència i Nanotecnologia (IN2UB), Universitat de Barcelona, 08028 Barcelona, Spain*

[4]*Alba Synchrotron Light Facility, CELLS, Barcelona, Spain*

(Received 12 May 2017; revised manuscript received 29 June 2017; published 11 September 2017)

We present experimental evidence of transverse magnetic domains, previously observed only in nanostrips, in CoNi cylindrical nanowires with designed crystal symmetry and tailored magnetic anisotropy. The transverse domains are found together with more conventional vortex domains along the same cylindrical nanowire, denoting a bistable system with similar energies. The surface and the inner magnetization distribution in both types of domains are analyzed by photoemission electron microscopy with x-ray magnetic circular dichroism contrast, and hysteresis loop in individual nanowires are measured by magneto-optical Kerr effect. These experimental data are understood and compared with complementary micromagnetic simulations.

DOI: 10.1103/PhysRevB.96.125415

I. INTRODUCTION

Magnetic domains and the magnetization reversal in ferromagnetic cylinders are classical topics in nanomagnetism where geometry by itself leads to unique consequences. The high aspect ratio defines a magnetic shape anisotropy which promotes longitudinal domains. On the other hand, the circular symmetry often enables less common domains where magnetic moments are not aligned parallel to each other but follow a circumferential path. All these peculiarities are even more pronounced in nanoscale wires.

Cylindrical magnetic nanowires (NWs) as single nanostructures or as part of three-dimensional ordered architectures are considered for applications in nanotechnology areas, such as magnetic recording, microwave devices, functionalization for biomagnetics, and, more recently, for thermomagnetoelectric devices [1–3]. They are proposed in spintronics as alternatives to planar nanostrips owing to their specific advantages, such as the possibility to tailor the type of domain wall (DW) by adjusting the geometry [4], DW stability during motion [5], and the suppression of the Walker breakdown [6,7]. The synthesis of cylindrical NWs inside porous templates with engineered composition and geometry is achieved by an inexpensive electrochemical route [8].

All the mentioned technological applications rely on the understanding and control of the magnetic configurations of the individual magnetic units, determined by the composition through the balance among the geometrical shape, magnetocrystalline, and magnetoelastic anisotropies. Much less attention has been paid to individual nanowires owing to difficulties to release them properly from the template and to perform reliable experimental work, usually in expensive and/or unavailable techniques, especially considering the additional difficulties introduced by the circular cross section. Only very recently has interest been growing to search for the deeper understanding of the domain structure and domain-wall motion in cylindrical nanowires.

Experimental imaging of the surface magnetic state has previously been carried out at remanence or under an *in situ* applied magnetic field by magnetic force microscopy (MFM) [9] and magneto-optical Kerr effect (MOKE) [10]. In addition, electron holography supplies information of the magnetic flux distribution of the internal magnetic structure apart from the stray fields outside the nanowires [11,12]. These techniques have specifically been used to investigate the magnetization reversal mechanism by domain-wall nucleation and propagation in Fe-, Co-, and Ni-based nanowires (single element, alloys, or multisegmented) with various modulations in diameter or in composition.

The diagram of magnetic states as a function of the cylinder aspect ratio has been considered from a micromagnetic viewpoint which essentially consists of axial, transverse, and vortex states [13]. These diagrams show that the in-plane (transverse) magnetic state is favorable only for cylinders in the form of magnetic dots. Accordingly, the state diagram for long nanowires [14] reports only longitudinal (in NWs dominated by the shape anisotropy) and vortex (NWs with perpendicular magnetocrystalline anisotropy) domains. On the other hand, transverse domains (defined as areas where all magnetic moments are parallel to themselves and point on the plane perpendicular to the axis of the nanowire) frequently are observed in magnetic nanostrips [15–18]. However, in cylindrical nanowires, although they were mentioned in the literature [19,20], an unambiguous experimental proof of transverse domains is presented here. In the previous studies, the two-contrast MFM images of magnetic domains in Co nanowires are interpreted as transverse domains with the help of analytical modeling. Unfortunately, MFM does not provide direct information of the magnetization inside the wire as it mainly can distinguish the magnetic charges detected on the surface of the wire. In this case, different magnetic configurations can lead to similar charge distributions on the surface. The distorted vortex domains, for example, also produce two-contrast MFM images, see Ref. [21].

*Corresponding author: cristina.bran@icmm.csic.es

†Present address: IMDEA Nanociencia, C/Faraday, 9, 28049 Madrid, Spain.

Photoemission electron microscopy combined with x-ray magnetic circular dichroism [22] (XMCD-PEEM) recently has proved to be a unique technique to explore the magnetization configuration of individual cylindrical nanowires. Due to the partial transmission of a grazing incidence x-ray beam through the wire, the core magnetic state is mapped onto the substrate, providing simultaneous information of the magnetization distribution at the surface (direct photoemission from the wire) and inside the nanowires (photoemission from the substrate). XMCD-PEEM has successfully been employed to identify Bloch-point domain walls in permalloy nanowires characterized by axial domains [23]. Vortex domains with circumferential magnetization at the surface and longitudinal at the core very recently have been confirmed in Co nanowires [21].

In this paper we synthesized CoNi cylindrical nanowires with different Co contents and designed magnetocrystalline anisotropy. By analogy to nanostrips where perpendicular magnetic anisotropy is responsible for transverse domains, we are able to design such domains in cylindrical NWs. Such a magnetic domain structure could offer an alternative for high-density and three-dimensional data storage devices in advanced magnetic memories since it is preferable to more common vortex domains which almost do not create surface charges.

II. SYNTHESIS AND STRUCTURAL CHARACTERIZATION

CoNi NWs were prepared by filling self-assembled pores of anodic aluminum oxide (AAO) templates by electroplating. The templates were obtained by hard anodization in an oxalic aqueous solution ($0.3M$) containing 5 vol % ethanol at a constant temperature of 0 °C. During the anodization, a constant voltage of 80 V was applied first for 900 s to produce a protective aluminum oxide layer at the surface of the disk, which avoids breaking or burning effects during the subsequent hard anodization [24]. After that, the voltage was increased steadily (0.08 V/s) up to 130 V and kept constant for 3600 s. Nanopores with 120 nm in diameter and 60 μm in length thus were obtained. Afterwards, the residual Al and the alumina barrier layer at the bottom of the foils were chemically etched, and a Au layer was sputtered to serve later as an electrode for the final electroplating of the NWs. Co_xNi_{100-x} ($35 \leqslant x \leqslant 85$) alloy NWs were grown into the nanopores of AAO templates at room temperature by dc electrodeposition using the electrolytes: $0.12-0.09M$ $CoSO_4 + 0.063-0.084M$ $CoCl_2 + 0.057-0.095M NiSO_4 + 0.058-0.084M$ $NiCl_2 + 0.32M$ H_3BO_3 [24]. The *p*H value was kept constant at about 3.0. For MOKE, MFM, and XMCD-PEEM measurements the individual NWs were released from the membranes by dissolving the alumina using an aqueous solution composed of chromic oxide and phosphoric acid.

From scanning electron microscopy (SEM) [see Fig. 1(a)] measurements we determined the NW diameters to be about 120 nm and the respective lengths: $L = 8\,\mu$m ($Co_{35}Ni_{65}$), $L = 18\,\mu$m ($Co_{65}Ni_{35}$), and $L = 18\,\mu$m ($Co_{85}Ni_{15}$). The composition of NW alloys $Co_{35}Ni_{65}$, $Co_{65}Ni_{35}$, and $Co_{85}Ni_{15}$ was determined by energy-dispersive x-ray spectroscopy. The structural characterization was performed by XRD using a PANalytical X'pert Pro x-ray diffractometer in Bragg-Brentano geometry.

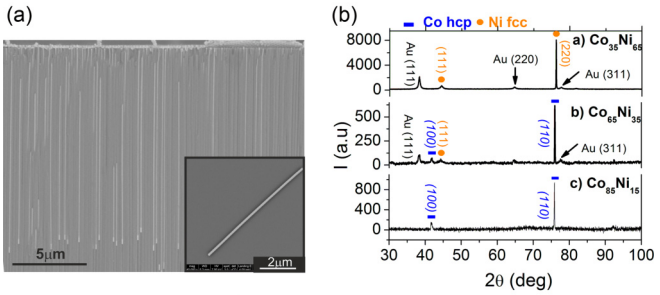

FIG. 1. (a) Cross-sectional SEM image of a CoNi NW array. The inset shows an individual NW on a Si substrate; (b) x-ray diffraction (XRD) spectra of arrays of Co_xNi_{100-x} NWs.

The XRD patterns of the AAO membranes filled with Co_xNi_{100-x} NWs are presented in Fig. 1(b). In $Co_{35}Ni_{65}$ NWs, Ni fcc (220) and (111) peaks are present. Additional peaks at 38.1°, 64.5°, and 77.5° belong to fcc Au sputtered on the back side of the sample. For $Co_{65}Ni_{35}$, the hcp phase with a (110) peak at 75.8° is detected as well as a smaller peak ascribed to (220) fcc Ni. In the case of $Co_{85}Ni_{15}$, only the hcp phase with (110) and (100) peaks is observed. A transition from the fcc structure for Ni-rich NWs towards the hcp hexagonal phase for a Co-rich alloy is thus concluded.

III. RESULTS AND DISCUSSIONS

A. Magnetic measurements of single nanowires

Longitudinal MOKE hysteresis loops of individual $Co_{85}Ni_{15}$ and $Co_{65}Ni_{35}$ nanowires, measured in a NanoMOKE™ 2 setup and shown in Fig. 2(a), were recorded under an applied field parallel to the nanowire axis. For the $Co_{85}Ni_{15}$ nanowire only a minor loop with reduced hysteresis and longitudinal susceptibility has been measured due to limitations of the maximum applied magnetic field in our setup. This magnetic behavior is consistent with the presence of a hcp crystalline phase with a strong magnetocrystalline anisotropy value causing the reorientation of the magnetization easy axis towards a nearly perpendicular orientation. In the case of $Co_{65}Ni_{35}$, a larger hysteresis is observed together with significant higher remanence. Figure 2(b) shows the simulated

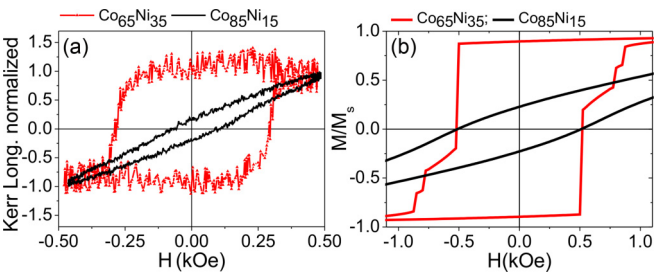

FIG. 2. (a) MOKE hysteresis loops of $Co_{85}Ni_{15}$ (black lines) and $Co_{65}Ni_{35}$ (red lines) nanowires under a magnetic field applied parallel to the nanowire axis; (b) simulated hysteresis cycles of $Co_{85}Ni_{15}$ (black lines) and $Co_{65}Ni_{35}$ (red lines) nanowires.

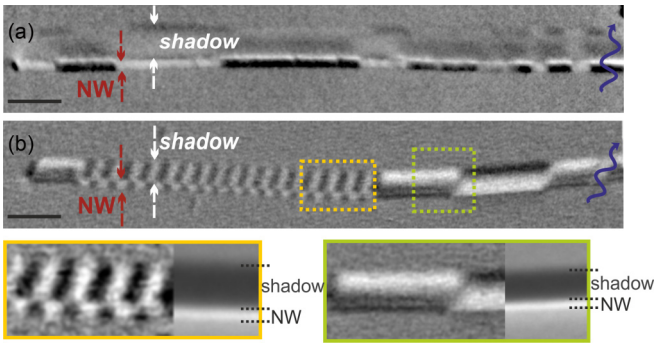

FIG. 3. XMCD-PEEM images of (a) $Co_{85}Ni_{15}$ and (b) $Co_{65}Ni_{35}$ nanowires. The scale bar is 1 μm, and the arrows (dark blue) indicate the incident x-ray beam. The inset figures at the bottom are enlarged images of the transverse and vortex domains in the corresponding regions of $Co_{65}Ni_{35}$. The right sides in the insets: Direct x-ray absorption (XAS) image of the same wire.

hysteresis loops for both $Co_{85}Ni_{15}$ and $Co_{65}Ni_{35}$ nanowires. Longitudinal MOKE hysteresis loops provide us with the first information on individual nanowires, although the data should be considered carefully as they are taken under a maximum field of 0.50 kOe, not large enough to magnetically saturate the samples. Consequently, a comparison between experimental data and simulations cannot be made straightforwardly.

XMCD-PEEM experiments were performed at the CIRCE beamline of the ALBA Synchrotron [25]. For Ni-rich nanowires ($Co_{35}Ni_{65}$), a highly uniform axially magnetized state is obtained at remanence (see Fig. S1 in the Supplemental Material [26]). Here, we focus on Co-rich nanowires where the images reveal the most interesting and complex magnetic domain structures. Figure 3 shows XMCD-PEEM images of individual $Co_{85}Ni_{15}$ and $Co_{65}Ni_{35}$ nanowires measured in a nearly perpendicular configuration of the x-ray propagation vector with respect to the nanowire axis. The marked regions of the images labeled as "NW" and "shadow," respectively, correspond to photoemission from the nanowire surface and that from the substrate after transmission through the wire core (see Fig. S2 in the Supplemental Material [26] for a schematic of the contrast modes of the surface/core).

In Figure 3(a), we observe two different magnetic contrasts along a $Co_{85}Ni_{15}$ nanowire. At the surface, it consists of alternating segments with opposite bright /dark contrast along the nanowire. Such an image indicates that the magnetic moments are oriented parallel and antiparallel, respectively, to the x-ray propagation vector, that is, perpendicular to the nanowire axis. The shadow contains segments with an opposite contrast to that of the wire (surface). The narrow strip of alternating bright/dark contrast observed at the upper edge with opposite contrast and same periodicity as that of the image obtained in direct photoemission corresponds to transmitted photons through the top surface of the nanowire. Notice that, for the same magnetic moment orientation, opposite contrast is expected between direct and transmitted signals (see Fig. S2 in the Supplemental Material [26]). From the bright/dark pattern of the whole shadow, the presence of vortex domains structure with alternating chirality along the nanowire surface is concluded, similar to those observed in Co nanowires [21]. Note that the length of such vortex domains is not constant along the nanowire.

However, the most striking configurations are observed for a $Co_{65}Ni_{35}$ nanowire where the magnetic contrast at the surface shows two different regions. This is depicted in Fig. 3(b) where the XAS images are used as a reference to correlate the position of the wire and the shadow.

(i) On the right side of the wire, a sequence of segments with opposite contrast similar to those in Fig. 3(a) is observed. The shadow consists of segments with an opposite contrast to that of the wire (surface) and increasing intensity as the edge of the wire is reached (see the inset), indicating that the circular magnetization pattern penetrates nearly fully into the nanowire. Thus, we conclude the presence of vortex domains with alternating chirality. Again, their lengths are not constant along the nanowire.

(ii) On the left side of the wire, a regular sequence of segments with much shorter periodicity and alternating contrast (i.e., bright/dark at the surface and dark/bright in the core) is observed [20] [see also the inset in Fig. 3(b)]. The contrast in the shadow is opposite to that at the surface and remains constant in the transversal direction (see the inset), showing clearly that the magnetization state is homogenous along the complete circular cross section of the wire. This is clearly different from the typical vortex domains in Fig. 3(a), and it is interpreted to correspond to transverse domains with significant components of magnetization in the perpendicular direction to the nanowire axis and alternating orientation. The width of the observed transverse domains is estimated to be about 150 nm and very regular. Both can be understood to be a result of the large local stray field associated with a transverse domain which is compensated by alternating domains. Note that, in contrast, a vortex domain represents a flux closure state with little or no local stray field.

This hybrid domain structure, i.e., the coexistence of transverse and vortex domains in the same wire, anticipates that the local domain structure is not uniquely defined by the composition but is determined by very subtle energy differences, defining its metastable character.

B. Micromagnetic simulations

For a deeper understanding, micromagnetic simulations of cylindrical nanowires were performed using the MUMAX3 code [27] for Co_xNi_{1-x} alloy nanowires ($x = 85$, 65, and 35). Based on our experimental data, a polycrystalline fcc (111) cubic symmetry for $Co_{35}Ni_{65}$ and a single hcp crystal with an easy axis nearly perpendicular to the NW axis for $Co_{85}Ni_{15}$ nanowires have been considered. For intermediate $Co_{65}Ni_{35}$ composition, we took a hcp polycrystalline structure with a "c" axis at 65° with respect to the NW axis and randomly distributed azimuthal angle. The equilibrium state is obtained by relaxation from a starting random magnetic configuration as corresponding to an as-prepared state. Further details are given in the Supplemental Material [26].

The simulation results corresponding to one of the possible configurations for the $Co_{85}Ni_{15}$ nanowire is shown in Fig. 4(a) where the equilibrium state is formed by a nonsystematic distribution of vortex and transverse domains along the nanowire. The pattern consists of vortex domains with opposite

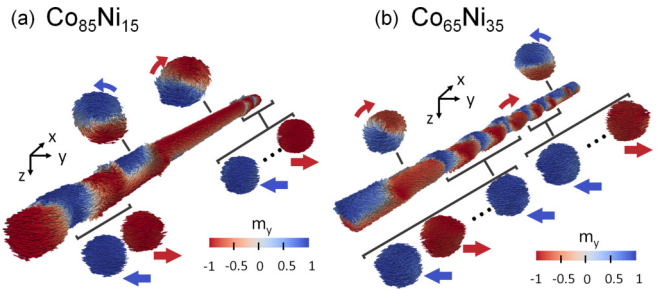

FIG. 4. Modeled magnetization configuration for (a) $Co_{85}Ni_{15}$ and (b) $Co_{65}Ni_{35}$ nanowires. The insets present the cross sections at the marked sites. The color scale shows the transverse component of magnetization.

chiralities and different lengths between shorter transverse domains with opposite directions close to the ends of the nanowire. The vortex structures extend over 68% of the nanowire. In short, the major section of the wire is formed by a vortex domain structure with random size and chirality distribution, similar to the XMCD-PEEM image shown in Fig. 3(a).

In the case of the $Co_{65}Ni_{35}$ nanowire [Fig. 4(b)] a more complex domain structure is obtained. Again, a hybrid magnetic structure of transverse and vortex domains is observed along the nanowire. However, now the transverse domains occupy a larger fractional volume, and the vortex domains mostly appear close to the ends. Around 52% of the nanowire length is filled by segments with opposite alternating transverse domains regularly distributed with an estimated length over 90 nm, notably close to the experimental data.

Overall, simulations reproduce remarkably well the experimental XMCD-PEEM data, although some points are not fully reflected. In $Co_{85}Ni_{15}$ nanowires, the simulated transverse domains were not observed experimentally. In $Co_{65}Ni_{35}$ nanowires, the hybrid system of transverse and vortex domains is well accounted for in the simulations, included the regular distribution transverse domains although their length, 90 nm in the simulation, is shorter than that found in the experiment, 150 nm. We also note that, in Fig. 3(b), the large zone with transverse domains changes into a vortex domain close to the left end of the wire, such as in simulations where vortices are found mainly at the end.

Vortex domain structures in hcp Co nanowires with almost perpendicular magnetocrystalline anisotropy have recently been reported to minimize the total magnetic energy [21]. Present simulations additionally predict the coexistence of vortices and transverse domains in alloy nanowires by tuning the magnetocrystalline anisotropy with the Co content of the alloy in the Co-rich case. That has fully been confirmed experimentally in the case of $Co_{65}Ni_{35}$ nanowires. The coexistence of the two kinds of domains actually reflects the metastable character of nanowires with multiple states of similar energies. For the simulations, fine-tuning of the saturation magnetization value, the exchange stiffness constant, and the magnetocrystalline anisotropy constant have been considered to reach the optimal fitting for experimental XMCD-PEEM data and the nano-MOKE loop.

The vortex structure essentially minimizes the magnetostatic energy, whereas the transverse one minimizes the exchange plus the anisotropy ones. The magnetostatic energy additionally is minimized by the creation of multiple domains along the nanowire. Since the $Co_{85}Ni_{15}$ has larger saturation magnetization (shape anisotropy energy density $K_{mag} \sim 510\,kJ/m^3$) than $Co_{65}Ni_{35}$ ($K_{mag} \sim 360\,kJ/m^3$), the formation of vortex domains is more favorable in $Co_{85}Ni_{15}$. However, one should also take into account that the anisotropy energy partly is minimized for the vortex domains by slight displacement of the core from the axial position [21]. Additionally, the domain walls between the vortex domains are more complex and require more exchange energy than those between the transverse domains. Consequently, the transverse domains become more favorable for a smaller value of the saturation magnetization. Since the magnetostatic energy is minimized almost completely by vortex domains, no additional minimization is needed, and the domains are much larger than in the transverse case.

IV. CONCLUSIONS

Metastable hybrid states of transverse and vortex domains are confirmed to coexist in the same CoNi nanowire. The transverse magnetic domains with homogeneous magnetization perpendicular to the nanowire axis as well as the vortex domains have been imaged by XMCD-PEEM. The data allow us to interpret the magnetization distribution at the surface and the inner region of the nanowires simultaneously. The coexistence of the metastable hybrid state is confirmed by micromagnetic simulations. The presence of the two types of domains in the same nanowire is understood considering the energy balance between transverse and vortex domain structures.

The design of transverse/vortex domains in cylindrical nanowires through suitable engineering of the magnetic anisotropy by small compositional changes opens an inexpensive route for high-density magnetic memories. The transverse domain states offer a novel alternative for advanced magnetic sensing and recording with more potential than commonly observed vortex domains. First, the local stray field produced by transverse domains is stronger as compared to the vortex ones, which is important for reading the output signal. Second, due to the minimization of the magnetostatic energy the transverse domains have reduced wavelengths, consequently enabling a higher information density.

ACKNOWLEDGMENTS

The study has been performed under the framework of the Projects No. MAT2013-48054-C2-1-R, MAT2016-76824-C3-1-R, MAT-2015-68772-P, MAT2015-64110-C2-2-P supported by the MINECO from Spain and DURSI 2014SGR220 supported by the Catalan Government. J.A.F.-R. acknowledges financial support from MINECO and the ESF through the "Ayudas para contratos predoctorales para la formación de doctores 2014." The PEEM experiments were performed at the CIRCE beamline of the ALBA Synchrotron with the collaboration of the ALBA staff.

[1] N. Shamsudhin, Y. Tao, J. Sort, B. Jang, C. L. Degen, B. J. Nelson, and S. Pané, Magnetometry of individual polycrystalline ferromagnetic nanowires, Small **12**, 6363 (2016).

[2] D. J. Lee, E. Kim, D. Kim, J. Park, and S. Hong, Nano-storage wires, ACS Nano **7**, 6906 (2013).

[3] J.-S. Kim, M.-A. Mawass, A. Bisig, B. Krüger, R. M. Reeve, T. Schulz, F. Büttner, J. Yoon, C.-Y. You, M. Weigand, H. Stoll, G. Schuütz, H. J. M. Swagten, B. Koopmans, S. Eisebitt, and M. Kläui, Synchronous precessional motion of multiple domain walls in a ferromagnetic nanowire by perpendicular field pulses, Nat. Commun. **5**, 3429 (2014).

[4] R. Hertel and J. Kirschner, Magnetization reversal dynamics in nickel nanowires, Physica B **343**, 206 (2004).

[5] R. Wieser, E. Y. Vedmedenko, P. Weinberger, and R. Wiesendanger, Current-driven domain wall motion in cylindrical nanowires, Phys. Rev. B **82**, 144430 (2010).

[6] H. Forster, T. Schrefl, D. Suess, W. Scholz, V. Tsiantos, R. Dittrich, and J. Fidler, Domain wall motion in nanowires using moving grids, J. Appl. Phys. **91**, 6914 (2002).

[7] M. Yan, A. Kákay, S. Gliga, and R. Hertel, Beating the Walker Limit with Massless Domain Walls in Cylindrical Nanowires, Phys. Rev. Lett. **104**, 057201 (2010).

[8] W. Lee, R. Ji, U. Gösele, and K. Nielsch, Fast fabrication of long-range ordered porous alumina membranes by hard anodization, Nat. Mater. **5**, 741 (2006).

[9] E. Berganza, C. Bran, M. Jaafar, M. Vázquez, and A. Asenjo, Domain wall pinning in FeCoCu bamboo-like nanowires, Sci. Rep. **6**, 29702 (2016).

[10] E. M. Palmero, C. Bran, R. P. Del Real, and M. Vázquez, Vortex domain wall propagation in periodically modulated diameter FeCoCu nanowire as determined by the magneto-optical kerr effect, Nanotechnology **26**, 461001 (2015).

[11] P. A. Midgley and R. E. Dunin-Borkowski, Electron tomography and holography in materials science, Nat. Mater. **8**, 271 (2009).

[12] L. A. Rodríguez, C. Bran, D. Reyes, E. Berganza, M. Vázquez, C. Gatel, E. Snoeck, and A. Asenjo, Quantitative nanoscale magnetic study of isolated diameter-modulated FeCoCu nanowires, ACS Nano **10**, 9669 (2016).

[13] F. Porrati and M. Huth, Diagram of the states in arrays of iron nanocylinders, Appl. Phys. Lett. **85**, 3157 (2004).

[14] Y. P. Ivanov, M. Vázquez, and O. Chubykalo-Fesenko, Magnetic reversal modes in cylindrical Nanowires, J. Phys. D: Appl. Phys. **46**, 485001 (2013).

[15] G. Leaf, H. Kaper, M. Yan, V. Novosad, P. Vavassori, R. E. Camley, and M. Grimsditch, Dynamic Origin of Stripe Domains, Phys. Rev. Lett. **96**, 017201 (2006).

[16] U. Ruediger, J. Yu, S. Zhang, A. D. Kent, and S. S. P. Parkin, Negative Domain Wall Contribution to the Resistivity of Microfabricated Fe Wires, Phys. Rev. Lett. **80**, 5639 (1998).

[17] I. L. Prejbeanu, L. D. Buda, U. Ebels, M. Viret, C. Fermon, and K. Ounadjela, Domain structures in epitaxial [1010] Co wires, IEEE Trans. Magn. **37**, 2108 (2001).

[18] C. Hassel, S. Stienen, F. M. Römer, R. Meckenstock, G. Dumpich, and J. Lindner, Resistance of domain walls created by means of a magnetic force microscope in transversally magnetized epitaxial Fe wires, Appl. Phys. Lett. **95**, 032504 (2009).

[19] L. Belliard, J. Miltat, A. Thiaville, S. Dubois, J. L. Duvail, and L. Piraux, Observing magnetic nanowires by means of magnetic force microscopy, J. Magn. Magn. Mater. **190**, 1 (1999).

[20] Y. Henry, K. Ounadjela, L. Piraux, S. Dubois, J.-M. George, and J.-L. Duvail, Magnetic anisotropy and domain patterns in electrodeposited cobalt nanowires, Eur. Phys. J. B **20**, 35 (2001).

[21] C. Bran, E. Berganza, E. M. Palmero, J. A. Fernandez-Roldan, R. P. Del Real, L. Aballe, M. Foerster, A. Asenjo, A. Fraile Rodríguez, and M. Vazquez, Spin configuration of cylindrical bamboo-like magnetic nanowires, J. Mater. Chem. C **4**, 978 (2016).

[22] S. Anders, H. A. Padmore, R. M. Duarte, T. Renner, T. Stammler, A. Scholl, M. R. Scheinfein, J. Stöhr, L. Séve, and B. Sinkovic, Photoemission electron microscope for the study of magnetic materials, Rev. Sci. Instrum. **70**, 3973 (1999).

[23] S. Da Col, S. Jamet, N. Rougemaille, A. Locatelli, T. O. Mentes, B. Santos Burgos, R. Afid, M. Darques, L. Cagnon, J. C. Toussaint, and O. Fruchart, Observation of Bloch-point domain walls in cylindrical magnetic nanowires, Phys. Rev. B **89**, 180405(R) (2014).

[24] V. Vega, T. Böhnert, S. Martens, M. Waleczek, J. M. Montero-Moreno, D. Görlitz, V. M. Prida, and K. Nielsch, Tuning the magnetic anisotropy of Co–Ni nanowires: Comparison between single nanowires and nanowire arrays in hard-anodic aluminum oxide membranes, Nanotechnology **23**, 465709 (2012).

[25] L. Aballe, M. Foerster, E. Pellegrin, J. Nicolas, and S. Ferrer, The ALBA spectroscopic LEEM-PEEM experimental station: Layout and performance, J. Synchrotron Radiat. **22**, 745 (2015).

[26] See Supplemental Material at http://link.aps.org/supplemental/10.1103/PhysRevB.96.125415 for details about XMCD-PEEM measurements and micromagnetic simulations.

[27] A. Vansteenkiste, J. Leliaert, M. Dvornik, M. Helsen, F Garcia-Sanchez, and B. Van Waeyenberge, The design and verification of MuMax3, AIP Adv. **4**, 107133 (2014).